Structure and energetics of long-period tilt grain boundaries using an effective Hamiltonian

D. N. Pawaskar
Division of Engineering, Brown University, Providence, Rhode Island 02912

R. Miller
Department of Mechanical Engineering, University of Saskatchewan, Saskatoon, Canada S7N 5A9

R. Phillips
Division of Engineering, Brown University, Providence, Rhode Island 02912
(Received 25 September 2000; published 10 May 2001)

We have investigated the atomic structures of 44 ⟨110⟩ symmetric tilt grain boundaries (GB's) with atomistic simulations using an embedded-atom method (EAM) potential for aluminum. The focus has been on examining the efficacy of the structural unit model in the context of very long period boundaries. Our studies, which have been carried out using two EAM potentials, of both the equilibrium and metastable structures of a number of boundaries, reveal that geometric arguments inherent in the structural unit model must be supplemented by energetic considerations. An effective Hamiltonian is introduced to this end which computes the energy of a string of structural units using two-body potentials between individual units. The potentials are calculated via a least-squares fit to the results of full atomistic represented by the effective Hamiltonian. Results based on as few as 16 inputs are very encouraging and clearly demonstrate the effectiveness of this method. This scheme lends itself to a straightforward extension to GB structure calculations at finite temperatures using Monte Carlo techniques.

DOI: 10.1103/PhysRevB.63.214105 PACS number(s): 61.72.Mm

I. INTRODUCTION

Grain boundaries (GB's) are ubiquitous in polycrystals and strongly affect their thermomechanical properties such as fracture toughness[1] and yield stress.[2,3] Interfacial motion via sliding[4] and migration,[5] which in turn are controlled by diffusion,[6] is an important mechanism which directly contributes to the macroscopic creep strain especially at elevated temperatures. These key properties become critical particularly in high-technology applications such as thin films in microelectronic devices and structural ceramics and composites.

Indeed, the intimate connection between structure and properties in a given material is often played out at the interfacial level. Ultimately, it is the atomic level structure of a boundary that will determine its motion and strength.[7] The study of atomic-level structure of grain boundaries has been greatly encouraged by the use of high-resolution transmission electron microscopy from which detailed information about the grain boundary geometry, defects and local atomic arrangement can be obtained. While many atomistic studies of GB structure have been performed,[8–10] they have often been confined to a number of special boundaries, such as simple symmetric tilt or twist boundaries with a high degree of symmetry and with a low Σ number. This has been primarily because of the fact that such boundaries exhibit special properties.[11] Also, the computational demands (memory and processor speed) involved in modeling such boundaries are relatively modest. However, it has been found that GB's which are not of this special type are also found in real microstructures. In fact, statistical surveys of distributions of types of boundary planes such as Ref. 12 have shown that such boundaries are more common than special boundaries. These include those with mixed tilt-twist character, boundaries for which no periodicity can be observed, boundaries which show steps and tiny facets with different misorientations, and those in which the GB plane wanders. In general, such boundaries have low periodicity and symmetry. While a great deal has been learned about GB deformation from the study of the simpler boundaries, extension to the more general configurations is essential to understanding how real materials behave.

In this paper, an effort is made to move in the direction of modeling very long-period boundary structures. The aim of this paper is twofold, the first being to improve the technique used in simulating long period grain boundaries. We also wish to address the problem of degeneracy of interface structures. In addition to the geometry of the misoriented crystals which constitute the GB, rigid body translations between them provide an important relaxation mechanism for minimizing the GB energy.[8] This leads to a wide variety of structures with different energies, often closely spaced, for the same misorientation angle and axis, which often exacerbates the task of picking out the equilibrium structure. The resolution of this thorny issue has been one of the major driving forces behind this project. We study symmetric tilt boundaries with ⟨110⟩ tilt axis since this class of boundaries is mot accessible to current high-resolution imaging techniques. This allows for the possibility that our calculations can be verified by experiments. Particularly attention is focused on those boundaries with very high Σ numbers (long periods). All calculations are carried out in the bicrystal setting and the structural unit model is used as a basis for our study. This geometric framework posits that a given grain boundary structure can be decomposed into a string of structural units as will be described in more detail below.

The remainder of the paper is organized as follows. Section II reviews ideas on GB geometry using the coincident site lattice formalism. The necessary details of the structural unit model are also presented in this section. We then explain the computational procedure to perform the GB structure calculations in Sec. III. We have looked at 32 different misorientations. Our calculations have revealed that in some cases the minimum energy structure does not jibe with expectations based on the structural unit model. This has been discussed in Sec. IV. In order to work around this discrepancy, we have proposed an effective Hamiltonian in Sec. V in which the energy of a GB is written as a cluster-expansion involving ''interaction potentials'' between different structural units. The effective Hamiltonian concept is particularly useful where permutations and combinations of objects (atoms, phases, stacking faults) give rise to configurations with different energies. Our calculations show that out of a given set of crystallographically equivalent grain boundary structures, the Hamiltonian can successfully pinpoint the minimum energy structure with a very high degree of accuracy. Section VI closes with a few reflections on both the merits and weaknesses of our approach.

II. CONCEPTUAL BACKGROUND

A. Grain boundary geometry

The geometry of a planar interface formed between two crystals can be uniquely described by five macroscopic parameters, namely, the boundary plane normal **n**, the axis of rotation **a**, and the rotation angle θ. In addition to these five degrees of freedom, three microscopic degrees of freedom are also associated with a given interface, these being the positions of the two crystals with respect to each other along the three coordinate axes. If $\mathbf{a}\cdot\mathbf{n}=0$, the GB is called a tilt boundary and if $\mathbf{a}\times\mathbf{n}=\mathbf{0}$, it is called a twist boundary. In addition, if **n** is the same in both grains, then the GB is said to be symmetric otherwise it is asymmetric. If the Miller indices of **n** are rational, the GB is said to be rational otherwise it is an irrational interface. The coincident site lattice[13] model describes the formation of a GB by rotating two crystals through each other about appropriate rotation axes and through discrete rotation angles which leads to some fraction of coincident sites between the two lattices. This implies that the boundary thus formed is periodic. An irrational boundary, however, is periodic in at most one direction.[14] The Σ number is the inverse fraction of the individual lattice sites which are common to the two adjoining grains and is used to quantify the degree of overlap. Since computer simulations of GB's almost always employ periodic boundary conditions, it is very difficult to model irrational interfaces as such. However, it is possible to approximate an irrational interface by a long-period GB and thus carry out the required analysis. The misorientation angle of an irrational interface is not a special angle which leads to a coincident lattice and the Σ of such a boundary is theoretically infinite. However, one can find an angle corresponding to a coincident lattice arbitrarily close to this ''irrational angle'' and hence a Σ number that is arbitrarily high. This follows from the fact that one can approximate an irrational number to any precision by a rational number p/q where p and q are arbitrarily high coprime integers.[15] It is important to note the difference between GB *geometry and structure*. Geometry refers to the macroscopic parameters which quantify the misorientation of the two abutting grains while by structure, a detailed specification of the local arrangement of the atoms which constitute the boundary is meant.

B. The structural unit model

As noted above, in addition to the macroscopic geometric parameters characterizing a boundary there are additional questions concerning the atomic positions near the interface. The structural unit model is a powerful tool in understanding the structure of pure tilt or twist grain boundaries. According to this model, the structure of a long period boundary can be described as a combination of structural units found in two shorter period boundaries. This idea has been extensively developed in Ref. 9. The model allows one to predict the structure of a boundary of any misorientation angle for a given tilt axis and boundary plane, provided that one knows the structural details of two short period boundaries. These short period boundaries are also known as *favored boundaries* because they are special low-energy boundaries whose structure is a repeating string of short identical units. These boundaries are also called *delimiting boundaries*, as they delimit a range of misorientation angles. The contention of the structural unit model is that any boundary whose misorientation angle lies in this range will have a structure that is a predictable pattern (linear combination) of the structural units found in the two delimiting boundaries. The algorithm, according to which the minority units are separated as much as possible, to determine the number and sequence of these units is detailed in Ref. 14.

For example, consider the tilt boundaries shown in Fig. 1. In frames (a), (b), and (c) three delimiting boundaries are shown. The solid lines indicate the structural units labeled as A, B, and C. Figure 2 shows these units in greater detail. The filled and empty circles represent the $abab\cdots$ stacking of atomic layers along the $\langle 110\rangle$ direction which is directed normal to the plane of the paper, with the different colors representing different depths into the page. The boundary in frame (a) is in fact just a perfect crystal (0°), but it is used to illustrate the origins of the A unit. The B and C units are seen in boundaries which have angles of tilt 31.59° and 50.48°, respectively. The indices $\langle ijk\rangle$ in Fig. 2 show the direction in which the arrow points. These indices are $\langle 110\rangle$, $\langle 552\rangle$, and $\langle 332\rangle$ for the A, B, and C units, respectively. Figure 3 shows a boundary whose misorientation angle (17.86°) lies between those of the delimiting boundaries A and B. The boundary structure (AAB) is seen to be made up of a mixture of A and B units. Thus, it is theoretically possible to predict the structure of any symmetric tilt boundary and confirm it through a computer simulation. The gist of the above discussion is that the structure of grain boundaries for the present purposes is reduced to the description of macroscopic geometric parameters and atomic positions constructed using the structural unit model. One of the key objectives of our work was to critically examine the limits and

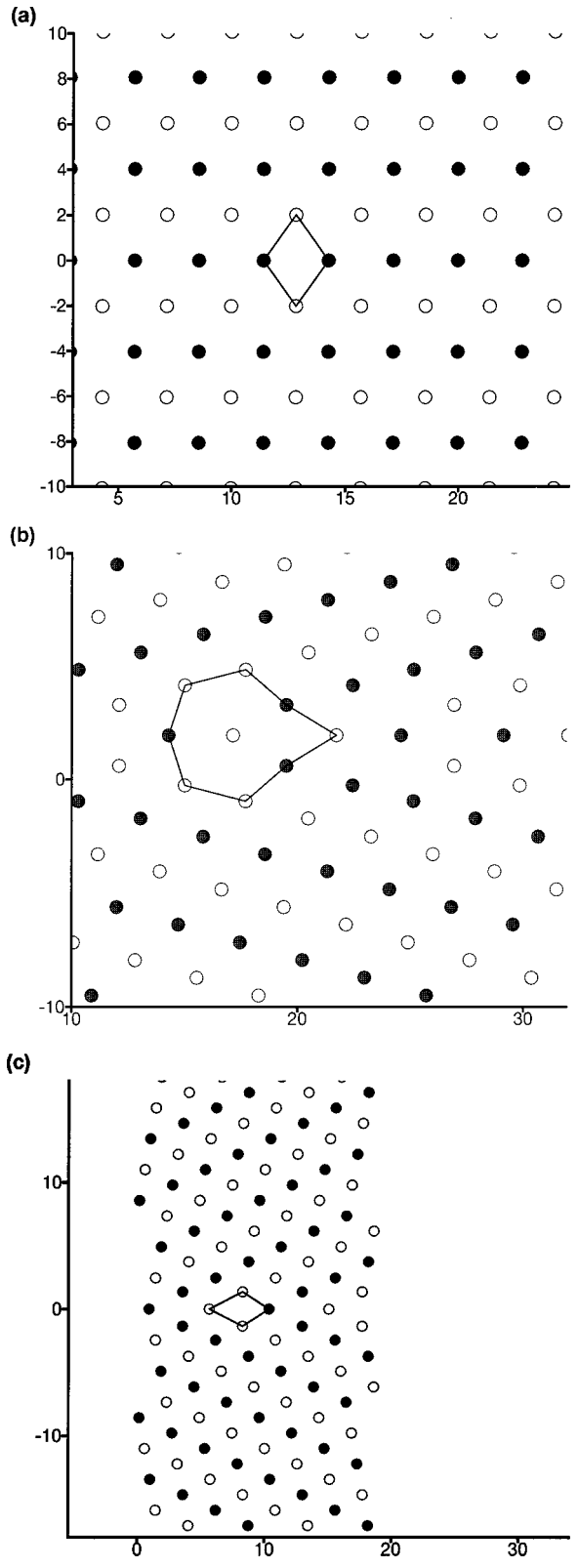

FIG. 1. Delimiting boundaries (a) $\Sigma 1(A)$, (b) $\Sigma 27(B)$, and (c) $\Sigma 11(C)$.

validity of these structural ideas. To do so, we have undertaken a suite of structural relaxations on a number of different long period boundaries. These relaxations allow for the determination of a series of a structural competitors at a given misorientation, and for an examination of the extent to which the minimum energy candidates correspond to the structures suggested by the structural unit model.

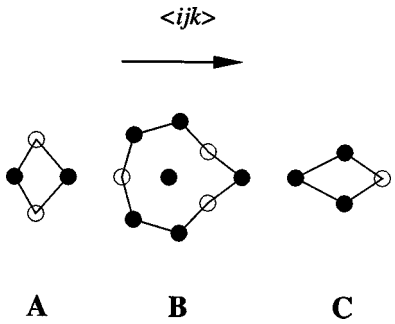

FIG. 2. Individual structure units.

III. COMPUTATIONAL PROCEDURE

In previous sections the necessity of studying the atomistic structure of interfaces was emphasized. We now detail the method used to calculate energies of GB structures at the atomic level.

A. Computational cell and force laws

The computational cell consists of a bicrystal as shown in Fig. 4. The boundary plane *XZ* is at the center of the cell. The atomic positions within the cell are generated using the coincident site lattice model. The total energy of the configuration is computed using the embedded atom method (EAM).[16] The total energy is then given by

$$E_{\mathrm{tot}}=\sum_i F_i(\rho_i)+\frac{1}{2}\sum_i \sum_{j\neq i} \Phi_{ij}(r_{ij}), \qquad (1)$$

where Φ_{ij} is a short-ranged pairwise interaction function and r_{ij} is the distance between atoms i and j. The total host electron density ρ_i at atom i is approximated as

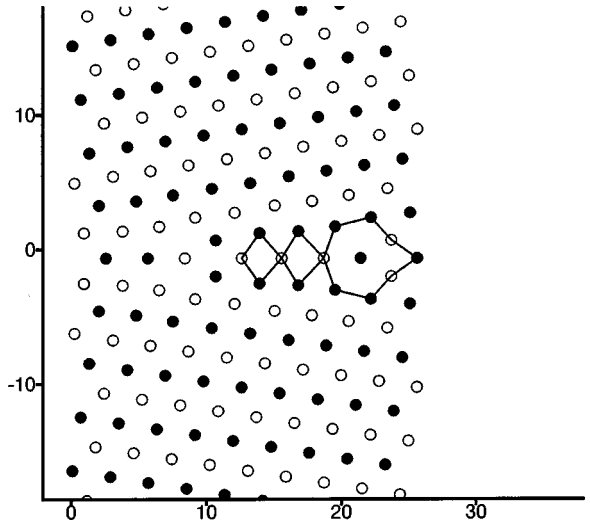

FIG. 3. Equilibrium structure of $\Sigma 83(AAB)$.

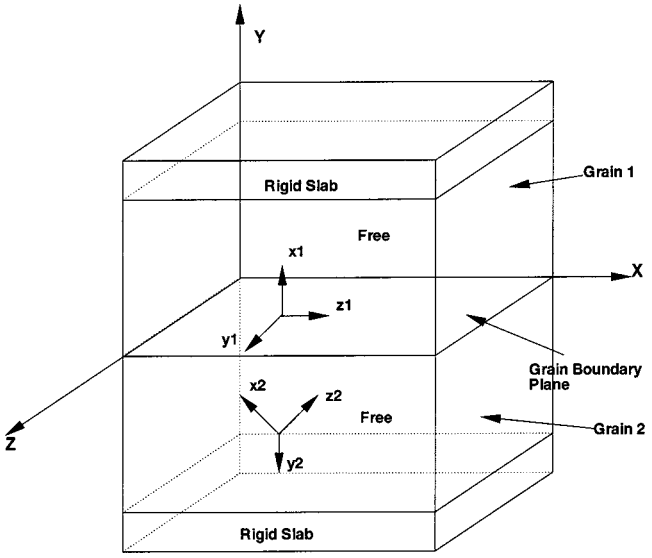

FIG. 4. Bicrystal computational cell.

$$\rho_i = \sum_{j \neq i} \rho_j(r_{ij}), \tag{2}$$

where ρ_{ij} is the contribution to the electronic density from atom j. Thus the energy is then a simple function of the atomic coordinates. For a given element, the three functions F, Φ, and ρ are fitted to experimental values or first-principles results or some combination of them both. Since the electron density terms are assumed to be radially symmetric, EAM potentials are best suited to modeling elements whose bonding is primarily nondirectional, such as the face-centered cubic (fcc) metals. Also, EAM potentials account for ''many body'' effects hence they are well suited to modeling defects such as interfaces, dislocations and surfaces where coordination effects are significant. EAM potentials have been widely used in modeling defects in metallic microstructures.[10] All calculations have been initially performed using the Ercolessi-Adams[17] EAM potentials for aluminum. For comparison, we have also used the Voter-Chen[18,19] potentials in some computations.

B. Boundary conditions

It should be clear from the context whether grain boundary or the *boundary* of the simulation cell is meant when the word boundary is used in this section. The simulation cell is periodic along the X and the Z axes in order to eliminate surface effects. Here, the Z axis is parallel to the tilt axis and the X axis lies in the grain boundary plane. In the Y direction (which is perpendicular to the grain boundary plane), the cell is divided into a ''free'' region and two ''rigid slab'' regions. The atoms on either side of the GB are in the free region, and they are sandwiched between two rigid blocks of perfect crystal. The atoms in the free region are allowed to individually move as a part of the relaxation process while those within each fixed region move as a single unit. Hence, only three translational degrees of freedom are associated with each rigid slab even though they contain on the order of 1000 atoms. Because the rigid slabs are at least twice as thick as the range of the atomic potentials used, the atoms in the free region essentially behave as though they were surrounded by two semi-infinite perfect crystals. The usual technique is to use periodic boundary conditions along all three directions. In other studies,[10] a simulation cell with two equivalent tilt boundaries, one at the middle of the cell and one on the border in the Y direction was built. Our method considerably cuts down the computational cost by reducing the number of effective degrees of freedom. It also allows for modeling asymmetric boundaries and ensures volumetric expansion in the direction perpendicular to the grain boundary plane. The energy minimization is carried out using a conjugate gradient algorithm, where the forces on the two rigid blocks were computed as the derivatives of the total energy with respect to each of the rigid block's translational degrees of freedom. When using this method of relaxation, it is important that the dimension of the simulation cell in the Y direction be large enough so that the strain in the crystal due to relaxation at the GB has essentially vanished at the interface with the two rigid blocks.

C. Rigid body translations

It is well known[20,21] that lattice statics energy minimization of GB's can lead to many different boundary structures depending on the initial configuration of the two grains. This is due to the multiwelled nature of the energy function in configuration space. Thus, for each macroscopically defined GB geometry, there are multiple microscopic GB structures that correspond to a number of local minima on the energy surface. The standard procedure to locate these minima involves the introduction of a relative displacement between the two grains along the boundary plane prior to relaxation. The global energy minimum and hence the associated structure is then chosen from the set of local minima by doing an exhaustive search. However, it is always possible to miss the true global minimum, as the approach takes a finite sample of an infinite number of possible initial configurations. For periodic boundaries, it has been shown[9] that it is possible to represent all possible initial configurations by the infinite set of points in the so-called *cell of nonidentical displacements*. The GB plane is periodic in the two mutually orthogonal directions (which lie in the plane). Hence, the GB structure repeats itself if one traverses a distance greater than the periodic length in the GB plane. By taking a reasonably fine grid of initial configurations from within this cell (of minimal periodicity) one can be fairly confident of achieving the global minimum energy structure. We have found that a grid spacing of about 1 Å in each direction (along $\mathbf{a}$ and $\mathbf{a}\times\mathbf{n}$) is sufficient. However, such a fine spacing considerably increases the computational time for high Σ boundaries since the period scales as $p \sim \sqrt{\Sigma}$. The plane of such boundaries has a very large area (on the order of 1000 Å^2). One way around this problem is to approximate the cell of the long-period boundary by that of an appropriate short period one and then use the corresponding displacements of the short period boundary as translations for the long period one. We propose an alternative method, which we refer to as the *small box technique*—use the displacements of the long period

TABLE I. Investigated misorientations.

No.	Group	Θ°	Σ	SUM pattern and other structures, if any
1	I	0.000	1	*A*
2	II	12.417	171	*AAAAB*
3		14.652	123	*AAAB*
4		17.860	83	*AAB*
5		19.263	643	*AABAABAB*
6		20.050	33	AABAB
7		20.553	1571	*ABAABABAABAB*
8		20.903	507	*ABAABAB*
9	III	22.844	51	*BA*[a]
10	IV	24.549	177	*BABBABA*
11		25.175	379	*BBABA*
12		25.699	1011	*BBABBABA*
13		26.525	19	*BBA*
14		28.026	307	*BBBA*[b]
15		28.840	129	*BBBBA*
16	V	31.586	27	*B*[a]
17	VI	34.179	579	*BBBBC*[b]
18		34.893	89	*BBBC*[b]
19		36.149	187	*BBC*[b]
20		36.810	321	*BBCBBCBC*[b]
21		37.219	491	*BBCBC*[b]
22		37.496	697	*BCBBCBCBBCBC*[b]
23		37.696	939	*BCBBCBC*[b]
24	VII	38.942	9	*CB*[a]
25	VIII	40.271	827	*CBCCBCB*
26		40.501	601	*CBCCBCBCCBCB*
27		40.827	411	*CCBCB*
28		41.325	257	*CCBCCBCB*
39		42.183	139	*CCB*
30		44.003	57	*CCCB*
31		45.169	339	*CCCCB*
32	IX	50.479	11	*C*

[a]Other structures also obtained

[b]SUM structure not the minimum energy structure.

boundary but by using a computational cell only a few cutoff radii thick and then use those displacements which yield low energies in this small unit cell as displacements for the original unit cell. Hence two steps are involved in this process: (1) use a cell with a small *Y* to find candidate initial guesses and (2) recompute those candidates that exhibit low energies using a cell with a larger *Y* to remove edge effects. We found this approach to be very effective in quickly identifying the translations which yield low energies. Since the length of the cell perpendicular to the GB plane is reduced in locating the low energy displacements, a considerable amount of computational time is saved. The origin of the plane containing the translations is shifted slightly above the boundary plane in order to break the initial symmetry of the bicrystal.

IV. EVALUATION OF LONG-PERIOD GRAIN BOUNDARY STRUCTURES

One way to analyze the structure of an irrational tilt boundary is to approximate that misorientation by a rational approximation with a very high Σ number. With this objective in mind, we have chosen to look at a wide range of misorientations shown in Table I. This selection is made such that a very broad range (1–1571) of Σ's were available and the majority of the boundaries were very long period ones. Also, all the three kinds of structural units (*A*,*B*,*C*) were present in the structures.

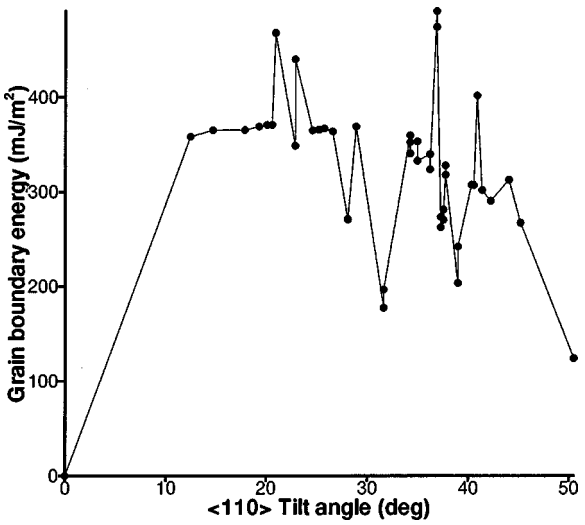

FIG. 5. Variation of grain boundary energy versus misorientation angle.

Figure 5 shows the variation of the grain boundary energy versus the misorientation angle. Note that for some angles, there are two or more values of energy. This is a consequence of finding more than one low-energy structure for some angles. The graph shows that for some angles, there are deep cusps in the energy which confirms the findings in Ref. 10. These minima in the energy correspond to a string of single unit structures as discussed earlier. However, we also find other cusps in the energy (both maxima and minima), which indicates local high- and low-energy structures associated with those energies.

For the purpose of this investigation, the boundaries can be classified into nine groups on the basis of their structures *as predicted by the structural unit model*. Each group represents a particular class of boundaries, the classification being made on the basis of the kinds of units present in them. In addition to providing taxonomical convenience, this classification is based upon the hypothesis that boundaries containing a characteristic structural string should exhibit special mechanical properties such as sliding strength or migration mobility. The three types of groups are as follows. (1) Those which contain only one type of structural unit, i.e., these groups contain the delimiting boundaries discussed earlier. Groups I, V, and IX fall into this category and they contain only one boundary each. (2) Those which contain only two types of structural units with equal numbers of each type. Again, these groups, III and VII, contain one boundary each. (2) Those which contain two different kinds of units but with an unequal number of the two units. All other groups other than the ones listed above can be categorized under this class. Since there is no limit to the number of structural units which form the boundaries in these groups, these groups

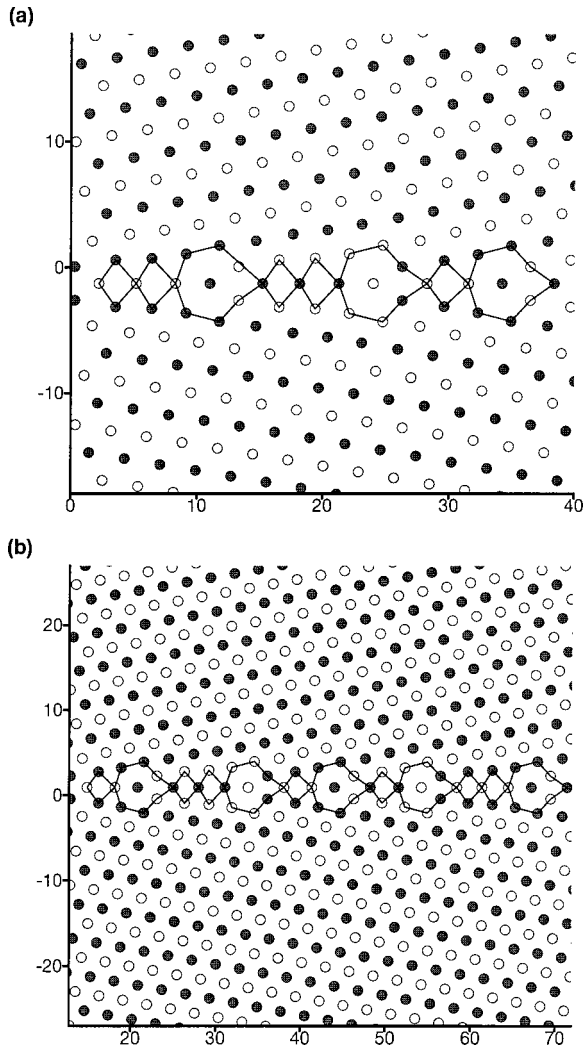

FIG. 6. Equilibrium structures of group II boundaries (a) $\Sigma 643(AABAABAB)$ and (b) $\Sigma 1571(ABAABABAABAB)$.

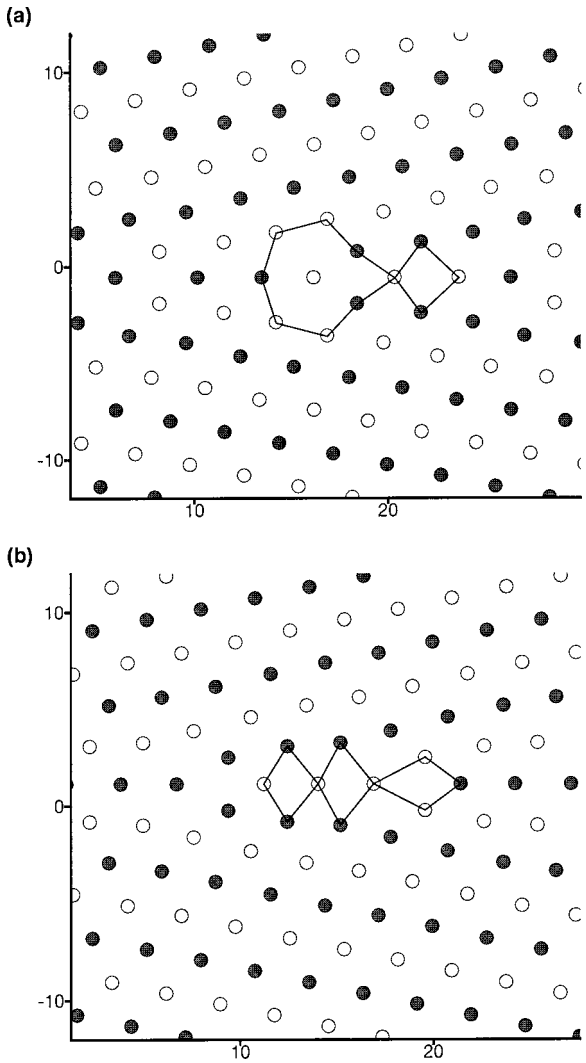

FIG. 7. Equilibrium structures of group III boundaries (a) $\Sigma 51(BA)$ and (b) $\Sigma 51(AAC)$.

contain infinitely many GB's. However, only a few examples of long-period boundaries from these groups are shown in Table I.

All the sequences of the structural strings in each boundary have been worked out according to the algorithm given in Ref. 14. Figures 1, 3, and 6–13 show the detailed structural details of some of the representative boundaries from each group. All dimensions shown are in Å.

A. Groups I–III

We now present a group-by-group investigation into the equilibrium and/or metastable structures obtained by minimizing all configurations corresponding to each misorientation from Table I. Group I contains only one boundary $\Sigma 1$ consisting of the *A* unit. This is shown in Fig. 1(a). The *A* unit corresponds to a perfect crystal with ''misorientation'' 0°. It is also a delimiting boundary. Group II contains structures which, according to the structural unit model, contain *A* and *B* units with the *A* units serving as the majority unit. We have shown two such long period structures in Fig. 6, namely, $\Sigma 643$ and $\Sigma 1571$ with structures *AABAABAB* and *ABAABABAABAB*, respectively. No other low-energy structures were obtained for any of these misorientations. Figure 7 shows two structures (*BA* and *AAC*) for the same Σ number. However, the lower-energy structure is the structural unit model prediction (*BA*) as expected.

B. Groups IV–VI

Group IV contains those boundaries whose structural unit model structures have an excess of *B* units compared to *A* units. Figure 8(a) shows the equilibrium structure (*BBABBABA*) of the $\Sigma 1011$ boundary. However, in the case of the $\Sigma 307$ boundary the minimum energy structure is not that predicted by the structural unit model which is *BBBA* [shown in Fig. 8(b)]. The structure which is obtained (*BBACA*) is shown in Fig. 8(c). This violation of the structural unit model is important because according to the model a boundary whose misorientations lies between those of its delimiting boundaries has a structure consisting of *two* types of units each belonging to the delimiting boundaries. This implies that more than two types of units cannot appear in

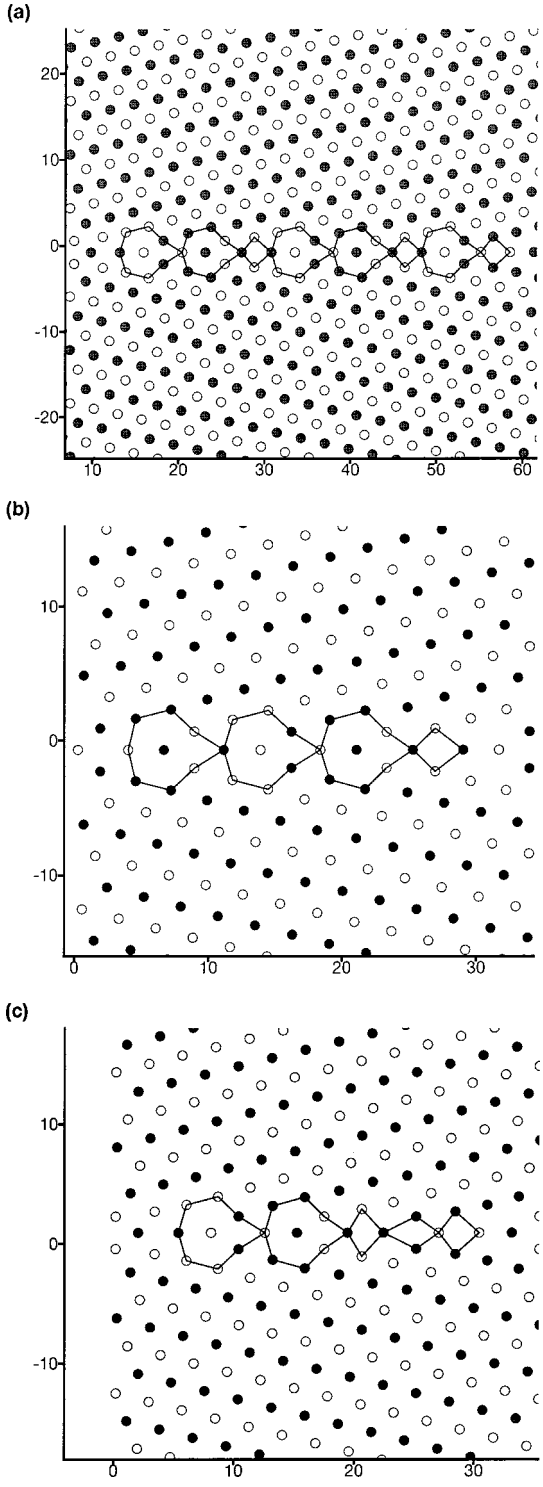

FIG. 8. Equilibrium structures of group IV boundaries (a) $\Sigma 1011(BBABBABA)$, (b) $\Sigma 307(BBBA)$, and (c) $\Sigma 307(BBACA)$.

the structure of a GB per the structural unit model. It is important to note that for these two boundaries, the two conflicting structures are crystal-lographically equivalent but energetically different. Also, the energy difference between the observed minimum energy structure and that predicted by the structural unit model is quite small (less than 5%). Group V contains a single misorientation corresponding to $\Sigma 27$ and

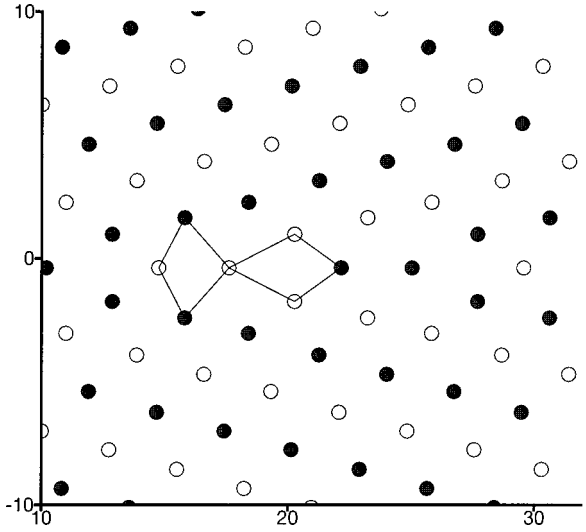

FIG. 9. Equilibrium structure of $\Sigma 27(AC)$ (group V).

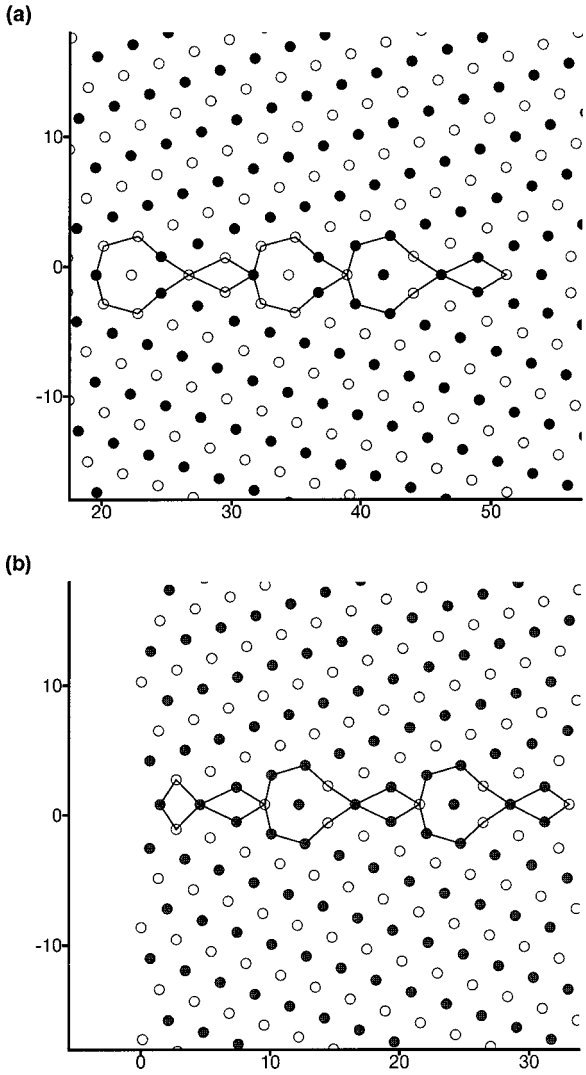

FIG. 10. Structural degeneracy in group VI boundaries (a) $\Sigma 491(BBCBC)$ and (b) $\Sigma 491(ACBCBC)$.

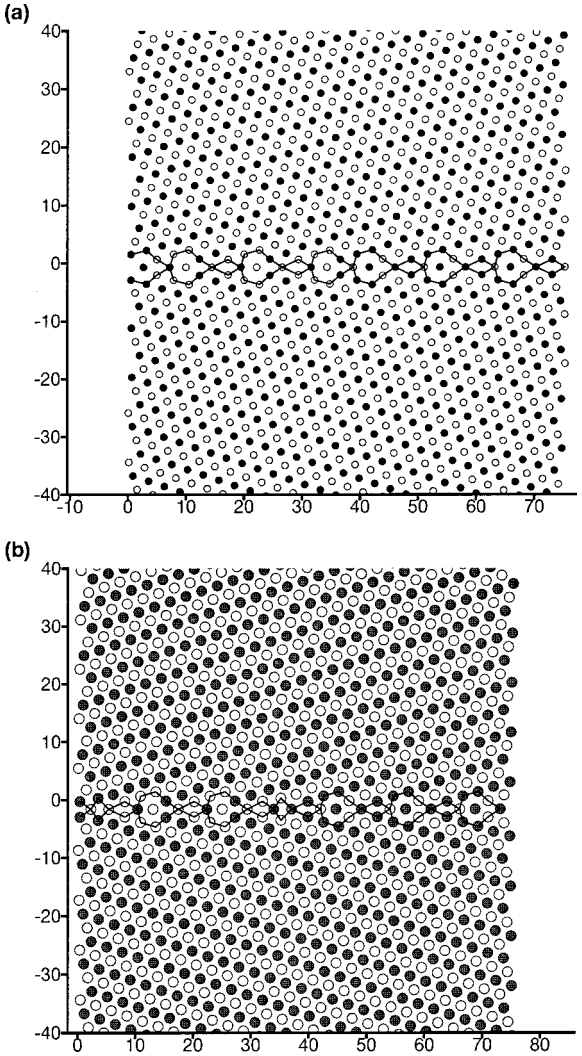

FIG. 11. Structural degeneracy in group VI boundaries (a) $\Sigma 697(BCBBCBCBBCBC)$ and (b) $\Sigma 697(CBCBCACBCBCBCA)$.

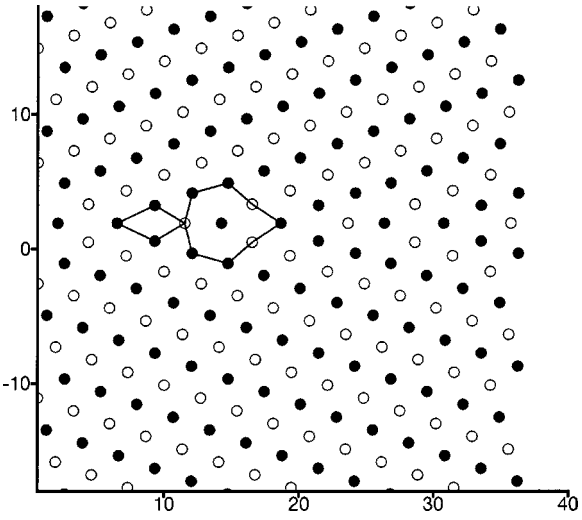

FIG. 12. Equilibrium structures of $\Sigma 9(CB)$ (group VII).

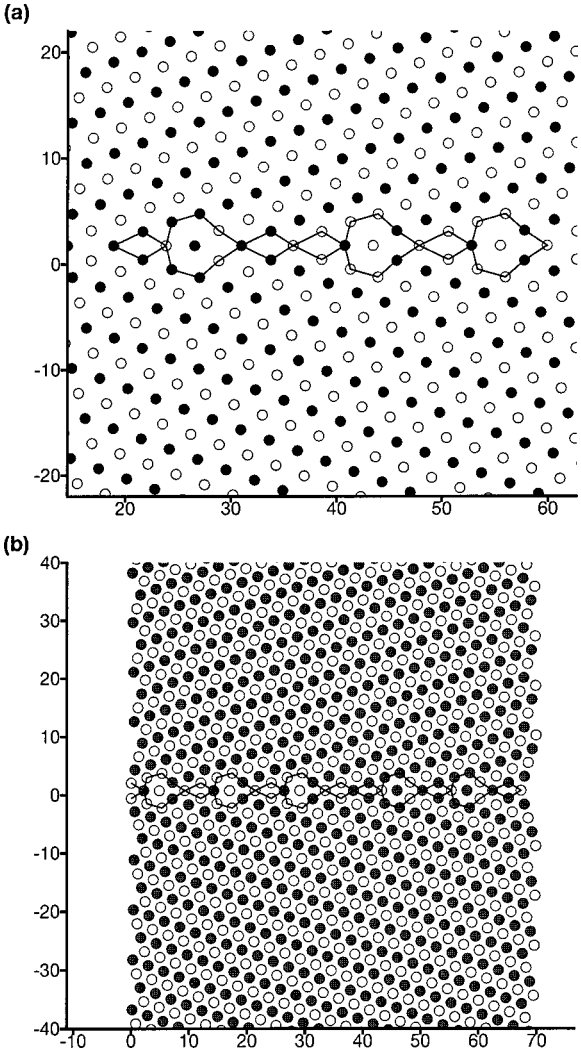

FIG. 13. Equilibrium structures of group VIII boundaries (a) $\Sigma 827(CBCCBCB)$ and (b) $\Sigma 601(CBCCBCBCCBCB)$.

the minimum energy structure is *B* which was already shown in Fig. 9. For this tilt angle, there is another structure *AC* (Fig. 9) which has higher energy than the *B* unit. Consequently, the *B* unit is a delimiting boundary as described earlier. For reasons which will be clear later, it was necessary to obtain the energy of the *AC* boundary.

Group VI is the most interesting case in this study. It contains misorientations whose structural unit model structures contain only *B* and *C* units, the *B* units being in a majority. Our simulations show that *none* of the boundaries in this group had an equilibrium structure according to that predicted by the structural unit model. In fact, the minimum energy structures obtained for these GB's show a violation of the structural unit model because they contain three different kinds of units. As examples of these occurrences we have shown two such structurally degenerate cases, namely, $\Sigma 491$ (Fig. 10) and $\Sigma 697$ (Fig. 11). The expected structure of $\Sigma 491$ boundary is *BBCBC* but the structure obtained is *ACBCBC*. Similarly, the conflicting structures of the $\Sigma 697$ boundary are *BCBBCBCBBCBC* and *CBCBCACBCBCBCBCA*. In all these cases, it is a *B* unit in the structural unit model struc-

ture that is replaced by the *CA* unit. It is worthwhile to note here that the tilt angle corresponding to the *B* unit is the same as that which corresponds to the *CA* unit. This discrepancy calls for a need to revise some of the details, energetics in particular, of the structural unit model. In general, our results justify the necessity of developing a scheme which can unambiguously predict the structure of a GB.

Our interpretation of the breakdown of the structural unit model is based on the ideal choice of delimiting boundaries. What this means is that if we choose the delimiting boundaries as those short-period boundaries which contain only one kind of structural unit (i.e., favored boundaries), the structural unit model is violated for some cases as shown in this paper. However, such a stringent choice of delimiting boundaries is not necessary according to Sutton.[14] If nonfavored boundaries are chosen, then the structural unit model may not be violated. Consider the boundary $\Sigma 307$ listed in Table II. Its structure as predicted by the structural unit model is *BBBA*. However, the lower-energy structure which we have obtained is *BBACA*. Now, if we choose $\Sigma 1$ (*A*) and $\Sigma 27$ (*B*) as its delimiting boundaries the obtained structure, *BBACA* does not obey the rules of the structural unit model and hence we claim a failure of the structural unit model. However if we choose $\Sigma 51$ (*AAC*) and $\Sigma 27$ (*B*) or $\Sigma 51$ (*BA*) and $\Sigma 27$ (*B*) as its delimiting boundaries the obtained structure *BBACA* does conform to the rules of the model. Thus the success or failure of the model depends to a large extent on the choice of delimiting boundaries. Of course, such a choice is not entirely arbitrary and is governed by the requirement that the structure of all boundaries in the misorientation range spanned by the delimiting boundaries is capable of being described as a linear combination of units found in the delimiting boundaries. This stipulation allows for some freedom in the choice of delimiting boundaries which may vary from group to group as well as for different boundaries within a group. Such a choice is also complicated by the requirement that the delimiting boundaries must be necessarily low-energy ones which implies that, in case of a conflict, one needs to know the energies of such boundaries in advance. In order to avoid such inconsistencies, we have sidelined these alternatives and applied a universal rule in the choice of delimiting boundaries—only those boundaries which contain one and only one kind of structural unit will be selected as delimiting boundaries. As we have seen earlier, the structural unit model is seen to fail in this framework. It is important to note that the effective Hamiltonian technique, presented later in the paper, is equally applicable to any choice(s) of delimiting boundaries and is thus a powerful method which can be used to predict interface structure.

TABLE II. Investigated structures.

No.	Σ	Structure
1	1	*A*
2	171	*AAAAB*
3	123	*AAAB*
4	83	*AAB*
5	643	*AABAABAB*
6	33	*AABAB*
7	1571	*ABAABABAABAB*
8	507	*ABAABAB*
9	51	*BA*[a]
10		*AAC*
11	177	*BABBABA*
12	379	*BBABA*
13	1011	*BBABBABA*
14	19	*BBA*
15	307	*BBBA*[b]
16		*BBACA*
17	129	*BBBBA*
18	27	*B*[a]
19		*AC*
20	579	*BBBBC*[b]
21		*ACDDDC*
22		*BACBBCBBBBC*
23	89	*BBBC*[b]
24		*ACBBC*
25	187	*BBC*[b]
26		*ACBC*
27	321	*BBCBBCBC*[b]
28		*ACBCACBCBC*
29	491	*BBCBC*[b]
30		*ACBCBC*
31	697	*BCBBCBCBBCBC*[b]
32		*CBCBCACBCBCBCBCA*
33	939	*BCBBCBC*[b]
34		*ACBCBCBC*
35	9	*CB*[a]
36		*ACC*
37	827	*CBCCBCB*
38	601	*CBCCBCBCCBCB*
39	411	*CCBCB*
40	257	*CCBCCBCB*
41	139	*CCB*
42	57	*CCCB*
43	339	*CCCCB*
44	11	*C*

[a]Other structures obtained.
[b]SUM structure not the minimum energy structure.

C. Groups VII–IX

$\Sigma 9$ is the sole member of group VII. Its structural unit model prediction is a structure *CB* which is also the minimum energy structure, as shown in Fig. 12. Group VIII contains boundaries with a majority of C units among B's. All the equilibrium structures in this class correctly follow the structural unit model rules. As an illustration, Fig. 13 shows two such structures $\Sigma 827$ (*CBCCBCB*) and $\Sigma 601$ (*CBCCBCBCCBCB*). The last group (group IX) has $\Sigma 11$ as its member and this structure (*C*) was already shown in Fig. 1

D. Effect of empirical potentials on grain boundary structures

The empirical potentials used in atomistic simulations can greatly influence the final results. For instance, the use of a

TABLE III. Effect of potentials on the failure of the structural unit model.

No.	Σ	Agreement with structural unit model: Ercolessi-Adams	Agreement with structural unit model: Voter-Chen
1	83	Yes	Yes
2	11	Yes	Yes
3	27	Yes	Yes
4	139	Yes	Yes
5	187	No	Yes
6	491	No	No
7	307	No	No
8	697	No	No
9	939	No	No

simple pair-potential returns no stacking fault energy in fcc aluminum. To begin to assess the role of our potentials in dictating the nature of our results, we have also used another EAM potential: the Voter-Chen potential as mentioned in an earlier section. In this context, we have addressed the following important questions.

(1) Does the use of a new EAM potential give rise to new (other than A, B, and C) structural units?

(2) If new structural units are not to be found, does the structural unit model break down in the same way as it did in the Ercolessi-Adams case?

(3) Are the actual energies of the relaxed structures close to those obtained by the Ercolessi-Adams potential?

First, we examine those boundaries which follow the structural unit model rules in the Ercolessi-Adams case. Only representative boundaries from each group are chosen for this purpose: Σ83, Σ11, Σ27, and Σ411. It is found that the relaxed structures (type of units and their combining sequence) of these boundaries are exactly the same as those obtained earlier. It should be pointed out here that the dimensions of the individual structural units do not match the earlier ones. This is because the Voter-Chen potential uses 4.05 Å as its lattice parameter for aluminum whereas that for the Ercolessi-Adams potential is 4.032 Å.

Next, we test five cases where structural unit model predictions did not hold earlier. Four out of the five such boundaries tested are from group VI since all the boundaries in this group fail the structural unit model. The only boundary not in group VI and which disobeys the structural unit model is the Σ307. Here, the minimum energy structure is *BBBA* as expected and this is the structural unit model prediction. For the boundaries from group VI, we find that the structural unit model breaks down in exactly the same way as in the Ercolessi-Adams case for Σ491, Σ697, and Σ939. The high Σ numbers of these boundaries should be noted here. However, the structural unit model prediction holds in the Σ187 case. These results are summarized in Table III.

We find that when the structural unit model prediction holds in the Ercolessi-Adams case, it also holds in the Voter-Chen case. The breakdown of the structural unit model is quite robust for both the potentials. This observation undoubtedly reinforces our case and calls for informing the structural units of their energetic roles. The next section describes how this is achieved by an effective Hamiltonian.

V. EFFECTIVE GRAIN BOUNDARY HAMILTONIAN

In the previous section we motivated the conception of a scheme to predict the minimum energy structure of grain boundaries. This involves augmenting the structural unit mode with requisite energetics in the present framework. One of the most powerful as well as popular techniques to compute energies of configurations involving permutations of their constituent elements is the use of cluster expansions. The ability of this method to describe the energetics and thermodynamics at finite temperatures when coupled with Monte Carlo techniques has been demonstrated in Refs. 21–24. The crux of the effective Hamiltonian method is to perform the computations over a reduced set of degrees of freedom associated with the system under investigation. For the GB's under consideration in the present study, the effective Hamiltonian assumes that the only effective degrees of freedom for the various GB structures are the structural units along the GB plane. The atomic coordinates of all other atoms are tacitly neglected. This results in a massive reduction in computational cost since now one does not have to track the other atoms which are not contained in the structural units. Their effects on the GB structure are accounted for by the interaction potentials between the structural units. Thus it it possible to determine the relaxed energies without having to determine the relaxed geometries, unlike traditional large-scale simulation methods such as molecular dynamics. Typical successful applications include but are not limited to stacking fault energies in aluminum[25] decoration in quasicrystals,[26] band structure and stability of semiconductor polytypes,[27] phase transitions in intermetallic solid solutions,[28] and oxygen ordering in YBCO superconductors.[29] Our idea is to assign energies to each structural sequence based upon the number of pairs of each type. To make this scheme useful, it it necessary to construct an effective Hamiltonian first.

A. The model

In this approach, we write the energy of a given boundary as the sum of the interaction energies of its constituent structural units. Thus,

$$E = E_0 + \frac{1}{2}\sum_{i=1}^{n}\sum_{j=-m}^{m}\Psi^{(j)}(s_i, s_{i+j}), \tag{3}$$

where E and E_0 are the energies of the simulation box with and without the GB, respectively. n is the total number of structural units in a given boundary, m is the maximum number of neighbors that participate in the energy interaction $\Psi^{(j)}(s_i, s_{i+j})$ is the two-body jth near-neighbor interaction between species s_i and s_{i+j} at sites i and $i+j$, respectively. The grain boundary energy γ is then given by

$$\gamma = \frac{E - E_0}{A} = \frac{\Delta E}{A}, \tag{4}$$

TABLE IV. Interaction types.

Interaction	q
A-A	1
A-B	2
A-C	3
B-B	4
B-C	5
C-C	6

where A is the area of the GB plane.

If the Ψ's are known, the energy of any configuration can be obtained simply by carrying out the above summation. One can then use this technique to determine the ground-state energy of a given structural string. The parameters Ψ are to be determined from a given (preferably as small as possible) set of configurations whose energy is directly available from atomistic simulations. If Ψ is to be computed to the mth near neighbor, this set should contain at least one structure which contains all interactions upto the mth near neighbor. Since at most three kinds of structural units, namely, A, B, and C are present in any of the boundaries under consideration, only six kinds of interactions are possible, namely, A-A, A-B, A-C, B-B, B-C, and C-C as shown in Table IV. The Hamiltonian can be split into summations over each number of neighbors to simplify the computation. The energy of a particular boundary k can now be rewritten as follows:

$$e_k = \sum_{i=1}^{n} N_{ik}\phi_i , \tag{5}$$

where $e_k = (E - E_0)_k$, n is a multiple of 6, and $i = (p-1)6 + q$ for the pth near-neighbor interaction of the qth type, p and q being integers. [If i is given, this Diophantine equation has the solution $q = \mathrm{mod}(i-1,6)$, $p = (i-q)/6+1$]. N_{ik} is a matrix whose entries are the numbers of first and second near-neighbors of each kind of interaction. This expression gives rise to a linear system of equations which is to be solved for the unknowns ϕ:

$$\mathbf{N}\phi = \mathbf{e}. \tag{6}$$

The following sample calculation example should serve to illustrate the effective Hamiltonian procedure. For the sake of simplicity, consider boundaries containing only A's and B's. So there are only three interactions (A-A, A-B, and B-B) involved. Assuming a first-near-neighbor model, we need to determine the three potentials ϕ_{AA}, ϕ_{AB}, ϕ_{BB}. One then needs to pick three boundaries, which contain all these interactions. Say, we pick AA, AB, and BB, the atomistic energies ΔE of which are 0.000, 0.631, and 0.465 eV. The energy of each of the three GB's can then be expressed as the following effective Hamiltonian expansion [Eq. (5)]:

$$e^{(1)} = N_{AA}^{(1)}\phi_{AA} + N_{AB}^{(1)}\phi_{AB} + N_{BB}^{(1)}\phi_{BB},$$

$$e^{(2)} = N_{AA}^{(2)}\phi_{AA} + N_{AB}^{(2)}\phi_{AB} + N_{BB}^{(2)}\phi_{BB},$$

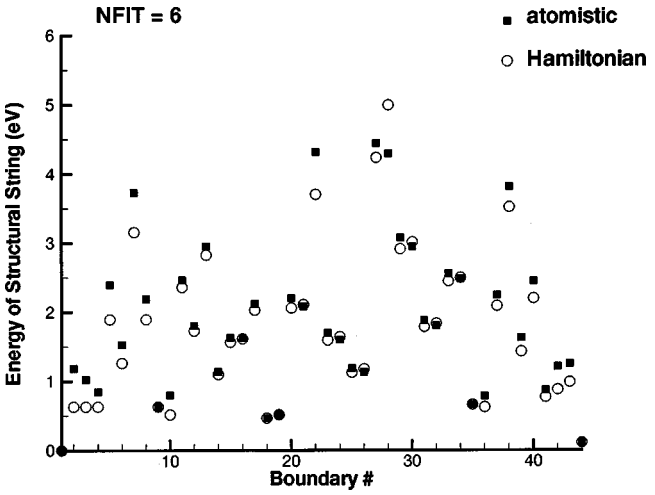

FIG. 14. Energy comparison using a direct fit using first near neighbor.

$$e^{(3)} = N_{AA}^{(3)}\phi_{AA} + N_{AB}^{(3)}\phi_{AB} + N_{BB}^{(3)}\phi_{BB},$$

where 1, 2, and 3 refer to the three GB's AA, AB, and BB, respectively, and $N_{AA}^{(1)}$ is the number of first-neighbor A-A interactions in GB 1, etc. The following linear system now needs to be solved:

$$\begin{pmatrix} 2 & 0 & 0 \\ 0 & 2 & 0 \\ 0 & 0 & 2 \end{pmatrix} \begin{pmatrix} \phi_{AA} \\ \phi_{AB} \\ \phi_{BB} \end{pmatrix} = \begin{pmatrix} 0.000 \\ 0.631 \\ 0.465 \end{pmatrix}.$$

The solution of which is $\phi_{AA} = 0.000$, $\phi_{AB} = 0.3155$, and $\phi_{BB} = 0.2325$.

B. Results and discussion

As a first step in determining the potentials ϕ, we assume only a first near-neighbor interaction between the units in a structural sequence, which gives rise to a 6×6 linear system as described by Eq. (6). Once the interactions have been obtained, the energies of all the structures can then be calculated using Eq. (5) and compared with the energies of these structures as obtained by atomistic calculations. Figure 14 shows a plot of these two energies. In order to be more quantitative about the quality of the fit, we have computed three key errors ε_1, ε_2, and ε_∞ which are the maximum positive percentage error, the root-mean-square percentage error and the maximum percentage error, respectively. The labels 1, 2, ∞ correspond to the familiar L_1, L_2, L_∞ norms. Also, as mentioned in an earlier section, one of goals of this project is to develop a generic scheme to identify a lower-energy structure out of a given set of crystallographically equivalent misorientations. Often, the rankings of the energies of different configurations is more important than the numerical values of the energies themselves since these values may be functions of the particular EAM potential in use. Thus, it is necessary to ensure that the fits return the same rankings of energies of crystallographically equivalent structures. To this end, we define a quantity g or ''goodness of a fit'' as the percentage of those boundaries with equal misori-

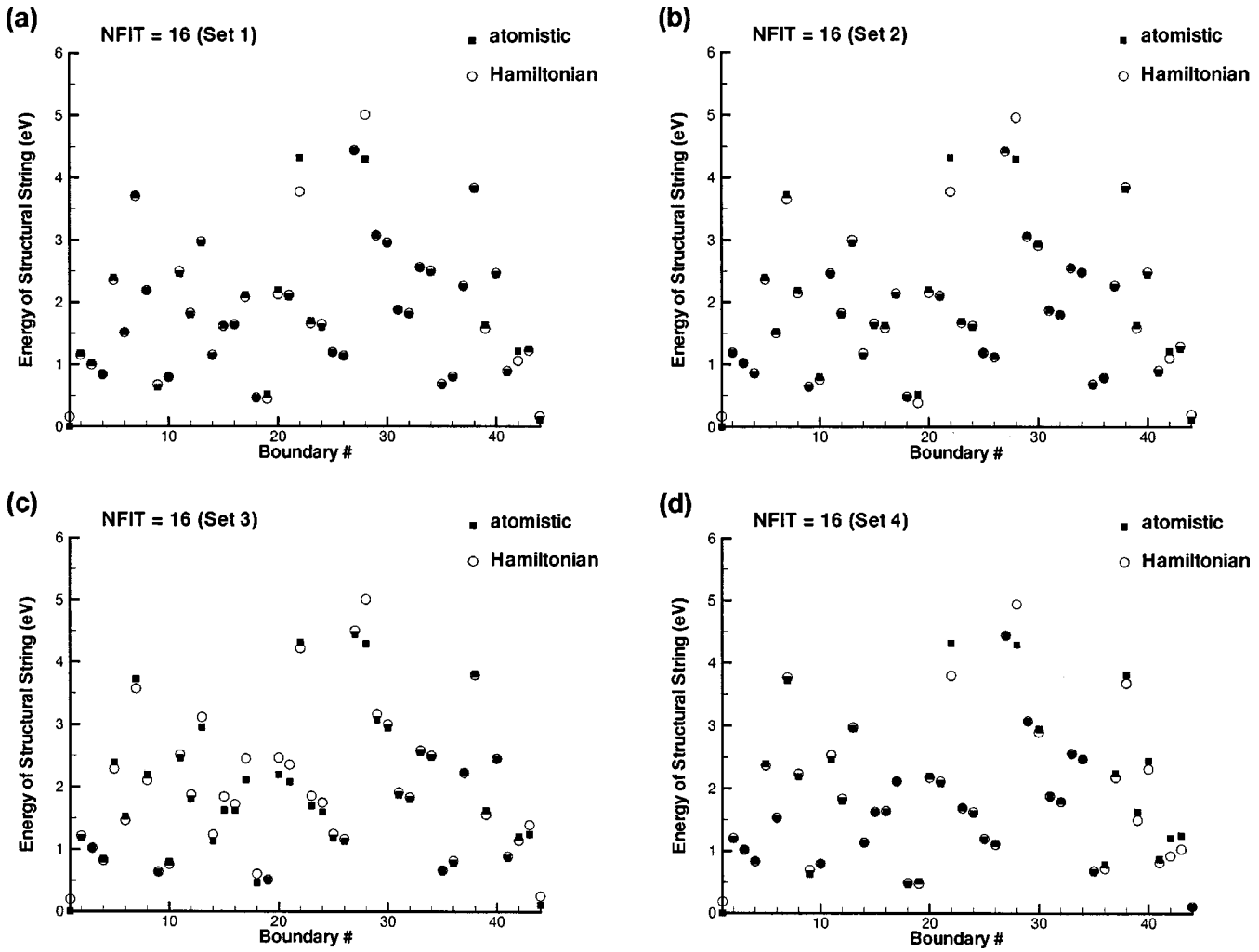

FIG. 15. Energy comparison using a second near-neighbor least-squares fit using different sets of 16 boundaries.

entations whose energy rankings have been preserved. Many of these boundaries are those which disobey the rules of the structural unit model. For the first near-neighbor fit $g = 23\%$ which calls for a significant improvement in the ability of the fit to (1) give energies very close to those already obtained via atomistic simulations, i.e., the errors ε_1, ε_2, and ε_∞ should be minimized and (2) preserve the energy rankings of GB's with equal misorientations, i.e., g should be maximized.

One way to ameliorate the fit is to increase the number of parameters involved in the energy computation and the most natural way to achieve this is to move to a second near-neighbor model which gives a 12-parameter Hamiltonian. The 12 parameters (potentials) are the solutions of the 12×12 system Eq. (6). However, we have been unable to find a set of 12 linearly independent equations, the coefficients of which are the numbers of a particular type of interaction. We believe that this is due to the extreme sparsity of the coefficient matrix **N**. To overcome this problem we have determined the 12 potentials by a least-squares fit instead of a direct fit. The least-squares equation is given by

$$\mathbf{N}\mathbf{N}^T\boldsymbol{\phi} = \mathbf{N}\mathbf{e}. \tag{7}$$

The least-squares analysis is carried out using a set of boundaries selected at random from the 44 different misorientations. Figures 15(a)–15(d) shows both the energies, obtained via atomistics and computed using the Hamiltonian, for all the boundaries using 16 ($NFIT = 16$) boundaries in the least-squares procedure. Considering the simplicity of the Hamiltonian as well as the number (as low as 16) of boundaries used to compute its parameters (16 in this case) the results are remarkably good. Figure 16 shows a similar fit with 32 boundaries, respectively. It is expected that in the second case, the fits would be more accurate since one is using more datapoints to compute the parameters. In order to quantitatively assess the accuracy of the fits, we refer to Table V which tabulates the average errors for the available fits. It can be seen that the average ε_1 error is almost equal for both $NFIT = 16$ and $NFIT = 32$. As expected, the average ε_2 and the ε_∞ errors are lower in the case of $NFIT = 32$. However, the average goodness g is higher for $NFIT = 16$. This is seemingly contradictory to expectations. But recall that the goodness g is a measure of the rankings of the energies. The least-squares algorithm minimizes only the overall error and is not required to maintain the rankings of the energies. This extra information could be, in theory, pro-

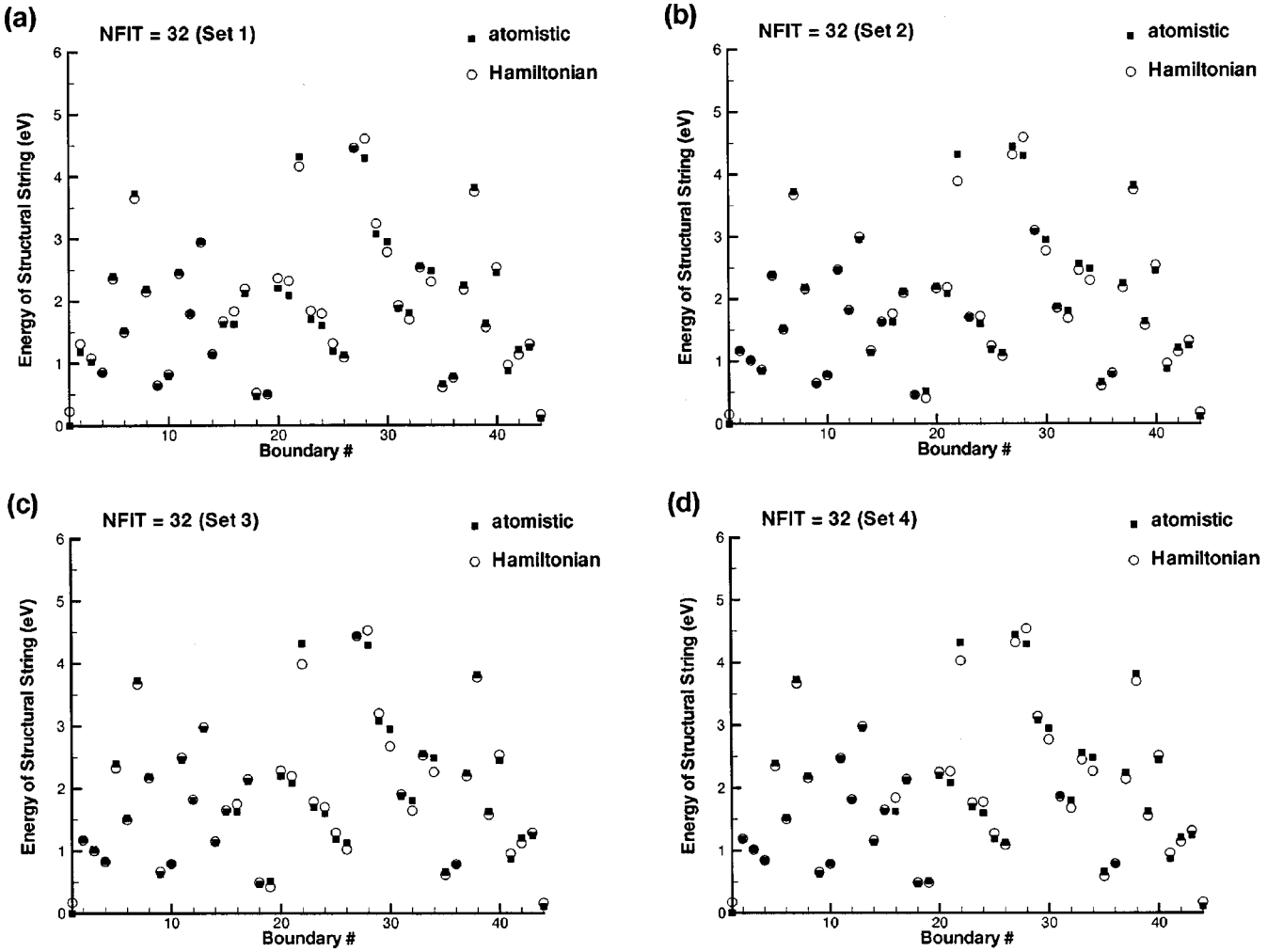

FIG. 16. Energy comparison using a second near-neighbor least-squares fit using different sets of 32 boundaries.

grammed into the least-squares method. This, however, is pointless because typically one does not *a priori* know the energy rankings.

An important issue that presents itself during the implementation of this method is which grain boundaries to use when computing the potentials. One has to decide whether to choose only simple structures, or the complex (long) ones, or a combination of both. Either way, there is a large degree of arbitrariness involved in making this choice. We have used a random selection of a particular number of grain boundaries in order to address this question. Figures 15 and 16 and Table VI show for a fixed number of boundaries, the fits are pretty robust as far as the errors are concerned. This is a positive feature because now the arbitrariness associated with the choice of GB's is removed to a certain extent. One need select a certain number of boundaries as inputs to the effective Hamiltonian and then compute the energies of other GB's.

TABLE V. Average errors.

NFIT	$\langle \varepsilon_1 \rangle$ %	$\langle \varepsilon_2 \rangle$ %	$\langle \varepsilon_\infty \rangle$ %	$\langle g \rangle$ %
16	5.00	12.50	72.00	80.76
32	5.48	10.54	59.00	69.23

VI. CONCLUSION

We have investigated 44 ⟨110⟩ symmetric tilt grain boundaries from the 0°–50.48° misorientation range with atomistic simulations using the embedded atom method. We have also carried out a detailed study of the resulting structures in the light of the structural unit model. The large num-

TABLE VI. Error analysis.

Fit. No.	NFIT	Set No.	ε_1 %	ε_2 %	ε_∞ %	g %
1	16	1	3.63	8.92	50.63	76.90
2	16	2	4.61	13.34	80.87	84.61
3	16	3	3.53	6.24	23.60	76.92
4	16	4	8.24	21.51	132.90	84.61
5	32	1	5.92	10.23	55.07	76.92
6	32	2	5.27	11.26	65.69	61.54
7	32	3	5.39	10.90	63.60	61.54
8	32	4	5.36	9.76	53.16	76.92

ber of possible rigid body translations in the GB plane gives rise to different structures even for boundaries with the same misorientation. We have also suggested two methods to reduce the computational time where the number of initial configurations is very large. The following conclusions have been reached as a result of this study.

(1) The large number of initial configurations (rigid body translations in the GB plane) make it very difficult to compute the structure(s) with a global energy minimum. However, this process may be simplified by implementing some of the techniques we have suggested.

(2) The competing structures for a given misorientation have their energies closely spaced—the energy difference being no more than 5%. Hence any model intended to predict the minimum energy structure should be sophisticated enough to pick out these small differences in energies.

(3) The structural unit model is a powerful tool for predicting the structures of even long-period boundaries. In many cases, nevertheless, our investigations have revealed the presence of structures with lower energies than those predicted by the structural unit model.

(4) In the instances where there is a multiplicity of structures for a particular boundary (misorientation) the lower-energy structures still consist of the structural units (*A*, *B*, *C*), however, in many cases their sequence violates the rules laid down by the structural unit model.

(5) The break-down of the structural unit model rules is seen particularly in high Σ boundaries. Also, it is reasonably insensitive to the particular type of EAM potential used. Our calculations with both the Ercolessi-Adams and the Voter-Chen EAM potentials have confirmed this observation.

(6) We have proposed an effective Hamiltonian as a complement to the existing structural unit model framework. The energy is computed using two-body interaction potentials between the individual units. The interaction potentials are determined by a least-squares fit.

(7) With energy inputs from as few as 16 boundaries, the Hamiltonian is able to reproduce the grain boundary energies to considerable accuracy. Also, it is capable of giving the correct rankings of the energies of competing structures. This feature is indispensable in picking out the minimum energy structure out of many low-energy configurations, of a particular grain boundary.

(8) The accuracy of the fits can be improved by incorporating more neighbors into the interactions and also by introducing many $(3+)$ body terms in the Hamiltonian. Also, it is fairly straightforward to extend the current investigation to finite temperatures by the use of Monte Carlo methods. The effect of applied stress on the evolution of GB structure can also be studied in this way.

ACKNOWLEDGMENTS

We thank M. Daw and S. Foiles for use of their DYNAMO code. We also thank C. Briant and A. Schwartzman for many useful discussions. This work was supported by the United States Department of Energy through Grant No. DE-FG02-96ER45578. This support is gratefully acknowledged.

[1] B. Ralph, in *Grain-Boundary Structure and Properties* (American Society For Metals, Metals Park, Ohio, 1979), p. 192.
[2] E. O. Hall, Proc. Phys. Soc. London, Sect. B **64**, 747 (1951).
[3] N. J. Petch, J. Iron Steel Inst., London **174**, 25 (1953).
[4] H. Kokawa, T. Watanabe, and S. Karashima, Philos. Mag. A **44**, 1239 (1981).
[5] A. H. King and D. A. Smith, Acta Crystallogr., Sect. A: Cryst. Phys., Diffr., Theor. Gen. Crystallogr. **36**, 335 (1980).
[6] J. P. Hirth, Metall. Trans. **3**, 3047 (1972).
[7] R. Phillips, *Crystals, Defects and Microstructures Modeling Across Scales* (Cambridge University Press, Cambridge, 2001).
[8] D. Wolf and K. L. Merkle, in *Materials Interfaces Atomic-level Structure and Properties*, edited by D. Wolf and S. Yip (Chapman and Hall, London, 1992).
[9] A. P. Sutton and V. Vitek, Philos. Trans. R. Soc. London, Ser. A **309**, 1 (1983).
[10] J. D. Rittner and D. N. Seidman, Phys. Rev. B **54**, 6999 (1996).
[11] G. Palumbo and K. T. Aust, in *Materials Interfaces Atomic-level Structure and Properties*, edited by D. Wolf and S. Yip (Chapman and Hall, London, 1992).
[12] V. Randle, Acta Mater. **46**, 1459 (1997).
[13] M. L. Kronberg and F. H. Wilson, Trans. AIME **185**, 50 (1949).
[14] A. P. Sutton, Acta Metall. **36**, 1291 (1988).
[15] W. Rudin, *Principles of Mathematical Analysis* (McGraw-Hill International Company, Singapore, 1984), p. 11.
[16] M. S. Daw and M. I. Baskes, Phys. Rev. Lett. **50**, 1285 (1983).
[17] F. Ercolessi and J. B. Adams, Europhys. Lett. **26**, 583 (1994).
[18] A. F. Voter and S. P. Chen, in *Characterization of Defects in Materials*, edited by R. W. Siegel, J. R. Weertman, and R. Sindair, MRS Symposia Proceedings No. 82 (Materials Research Society, Pittsburgh, 1987), p. 175.
[19] A. F. Voter and S. P. Chen, Intermetallic Compnd. Principles Practice **1**, 77 (1995).
[20] G. J. Wang, A. P. Sutton, and V. Vitek, Acta Metall. **32**, 1093 (1984).
[21] E. Tarnow, P. Dallot, P. D. Bristowe, and J. D. Joannopoulos, Phys. Rev. B **42**, 3644 (1990).
[22] J. M. Sanchez, F. Ducastelle, and D. Gratias, Physica A **128**, 334 (1984).
[23] J. W. D. Connolly and A. R. Williams, Phys. Rev. B **27**, 5169 (1983).
[24] C. Wolverton and A. Zunger, Phys. Rev. Lett. **75**, 3162 (1995).
[25] B. Hammer, K. W. Jacobsen, V. Milman, and M. C. Payne, J. Phys.: Condens. Matter **4**, 10453 (1992).
[26] M. Mihalkovic, W.-J. Zhu, C. L. Henley, and R. Phillips, Phys. Rev. B **53**, 9021 (1996).
[27] S-H. Wei, S. B. Zhang, and A. Zunger, Phys. Rev. B **59**, R2478 (1999).
[28] M. Asta and S. Foiles, Phys. Rev. B **53**, 2389 (1996).
[29] G. Ceder, Mol. Simul. **12**, 141 (1994).